



Influence analysis of complex crack geometric parameters on mechanical properties of soft rock

Yang Zhao¹ · Xin He¹ · Lishuai Jiang¹ · Zongke Wang¹ · Jianguo Ning² · Atsushi Sainoki³

Received: 29 May 2023 / Revised: 6 September 2023 / Accepted: 27 September 2023
© The Author(s) 2023

Abstract

Soft rocks, such as coal, are affected by sedimentary effects, and the surrounding rock mass of underground coal mines is generally soft and rich in joints and cracks. A clear and deep understanding of the relationship between crack geometric parameters and rock mechanics properties in cracked rock is greatly important to the design of engineering rock mass structures. In this study, computed tomography (CT) scanning was used to extract the internal crack network of coal specimens. Based on the crack size and dominant crack number, the parameters of crack area, volume, length, width, and angle were statistically analyzed by different sampling thresholds. In addition, the Pearson correlation coefficients between the crack parameters and uniaxial compression rock mechanics properties (uniaxial compressive strength UCS, elasticity modulus E) were calculated to quantitatively analyze the impact of each parameter. Furthermore, a method based on Pearson coefficients was used to grade the correlation between crack geometric parameters and rock mechanical properties to determine threshold values. The results indicated that the UCS and E of the specimens changed with the varied internal crack structures of the specimens, the crack parameters of area, volume, length and width all showed negative correlations with UCS and E , and the dominant crack played an important role both in weakening strength and stiffness. The crack parameters of the angle are all positively correlated with the UCS and E . More crack statistics can significantly improve the correlation between the parameters of the crack angle and the rock mechanics properties, and the statistics of the geometric parameters of at least 16 cracks or the area larger than 5 mm² are suggested for the analysis of complex cracked rock masses or physical reproduction using 3D printing. The results are validated and further analyzed with triaxial tests. The findings of this study have important reference value for future research regarding the accurate and efficient selection of a few cracks with a significant influence on the rock mechanical properties of surrounding rock mass structures in coal engineering.

Keywords CT scanning · Complex crack · Sampling threshold · Soft rock · Rock mechanics · Crack geometric parameters

1 Introduction

In most rock engineering cases, there are a large number of discontinuities (such as fissures, joints, and weak surfaces) in rocks because of geological movement and the tectonic

stress field (Jiang et al. 2016; Cao et al. 2016). Especially for soft rocks such as coal, which are affected by sedimentary effects, the surrounding rock mass of underground coal mines is generally soft and rich in joints and cracks (Kong et al. 2019; Gao et al. 2021). These discontinuities, joints, or cracks in the rock are widely believed to have a significant influence on the stability of the rock mass, particularly with regard to the following two aspects: (1) they decrease the strength and stiffness of the rock, and (2) they are a source of initiation of new discontinuities, which in turn may propagate and link with other cracks and further decrease the strength and stiffness of the rock (Wong and Einstein 2009; Bobet and Einstein 1998; Sagong and Bobet 2002). Therefore, understanding the relationship between crack geometric parameters and rock mechanical properties is important in coal engineering.

✉ Lishuai Jiang
lsjiang@sdust.edu.cn

¹ State Key Laboratory of Mining Disaster Prevention and Control, Shandong University of Science and Technology, Qingdao 266590, China

² College of Energy and Mining Engineering, Shandong University of Science and Technology, Qingdao 266590, China

³ Faculty of Advanced Science and Technology, Kumamoto University, Kumamoto 860-8555, Japan

Numerous rock laboratory tests and numerical simulation studies have been reported on the effects of crack geometric parameters on rock mechanical properties. For example, via numerical simulations, Cui et al. (2020) tested a particle model based on flat-joint and smooth-joint contacts to explore the effect of joint dip angle and joint spacing on the strength characteristics of rock under uniaxial compression with a set of nonpersistent open joints. Zhao et al. (2022) used a particle flow model to represent rock materials to investigate the relationship between the main microparameters (joint angle, length, density, and aperture) and uniaxial tensile strength; and Patel and Martin (2020) used a flat-jointed contact model to investigate the role of initial crack volume on the crack initiation stress of rock. By using laboratory tests, Li et al. (2019) produced preexisting joints in white marble by a high-pressure water cutting method to study the effect of the dip angles of joints on the rock dynamic mechanical properties, fracturing behavior, and energy evolution characteristics. In addition, 3D printing was used by Zhao et al. (2023) as a tool to examine the mechanical behavior of rock with discontinuities, and a control variable test was performed to investigate the effect of jointed geometric parameters (joint angle, length, and aperture) on the UCS and failure pattern. These studies indicate that the crack geometric parameters (joint angle, length, density, volume, aperture, etc.) have a very significant impact on rock mechanics properties. However, to date, few studies have been conducted to quantitatively analyze the correlation between crack geometric parameters and rock mechanics properties, even though a clear and deep understanding of this relationship in cracked rock is of great importance to the design of engineering rock mass structures.

Additionally, a large body of research has shown that the sampling interval, or sampling threshold, will greatly affect the crack morphology parameters (Xie et al. 1997; Xu et al. 2022). Furthermore, it will also undoubtedly have an impact on the correlation between crack geometric parameters and rock mechanics properties. Some researchers have shown that when the sampling interval of a crack surface meets a certain condition, the calculation results of the morphology parameters are very stable, and much research has been carried out to explore a reasonable sampling interval (Bao et al. 2020; Ge et al. 2021). However, there have been few reports about the effect of the sampling threshold on the correlation between crack geometric parameters and rock mechanics properties, which limits mechanical experimental investigations on complex crack rocks to a certain extent.

In this study, CT scanning was used to extract the internal crack network of coal specimens. Based on the crack size and dominant crack number, the parameters of crack area, volume, length, width, and angle were statistically analyzed by different sampling thresholds. In addition, the Pearson correlation coefficients between the crack parameters and

uniaxial compression rock mechanics properties (uniaxial compressive strength UCS, elasticity modulus E) were calculated to quantitatively analyze the impact of each parameter. Furthermore, the Pearson correlation coefficients were compared under different sampling thresholds, and the key parameters and the optimal threshold value were obtained. The results of this study will facilitate further research on the mechanical properties of rocks with complex cracks.

2 Extraction and analysis of crack network information based on CT scanning

2.1 The extraction of cracks

The Liangbaosi coal mine is located in Jining city, Shandong Province. The presence of softness and weak discontinuities (such as faults, joints or fractures) is consistent with the research objectives of this project (Zhu et al. 2021). Therefore, borehole core logging was conducted in the roof of the Liangbaosi coal mine, and specimens were obtained for the CT scanning tests. When X-rays emitted from an emission source pass through an object, the intensity of the X-rays is attenuated to some extent; the attenuation is influenced by the thickness and internal structure of the specimen. The attenuation characteristics follow the Lambert–Beer law, which is expressed as follows (Salamon et al. 2019; Zhou et al. 2016):

$$I = I_0 \exp(-\mu x) \quad (1)$$

where I is the intensity of X-rays after passing through the object, I_0 is the intensity of X-rays before passing through the object, μ is the attenuation coefficient of the sample being detected, and x is the penetration length of the incident X-rays.

The original grayscale CT image was binarized based on Otsu's method (Otsu et al. 1979). The black areas represent pores, and cracks can be easily identified and segmented from the solid matrix. In addition, the pores and cracks were assigned a value of 0, and the solid matrix was assigned a value of 1 (Huang et al. 2021; Omori et al. 2023). The pores and cracks can be divided from the scan slice one by one.

The X-ray 3D microscope nanoVoxel-4000 system of Tianjin Sanying Technology Company was used for the CT scanning measurements, and the CT device and the process of crack network reconstruction are shown in Fig. 1. The main parameters for the CT scanning tests include the following: the voltage = 150 kV, the current = 150 μ A, the exposure time = 0.8 s, the magnification = 4.6, the spatial separation rate = 0.127 mm, and the frame number = 1400/360°. The CT scanning data were first processed layer by layer to extract cracks. After the cracks were extracted, the slices

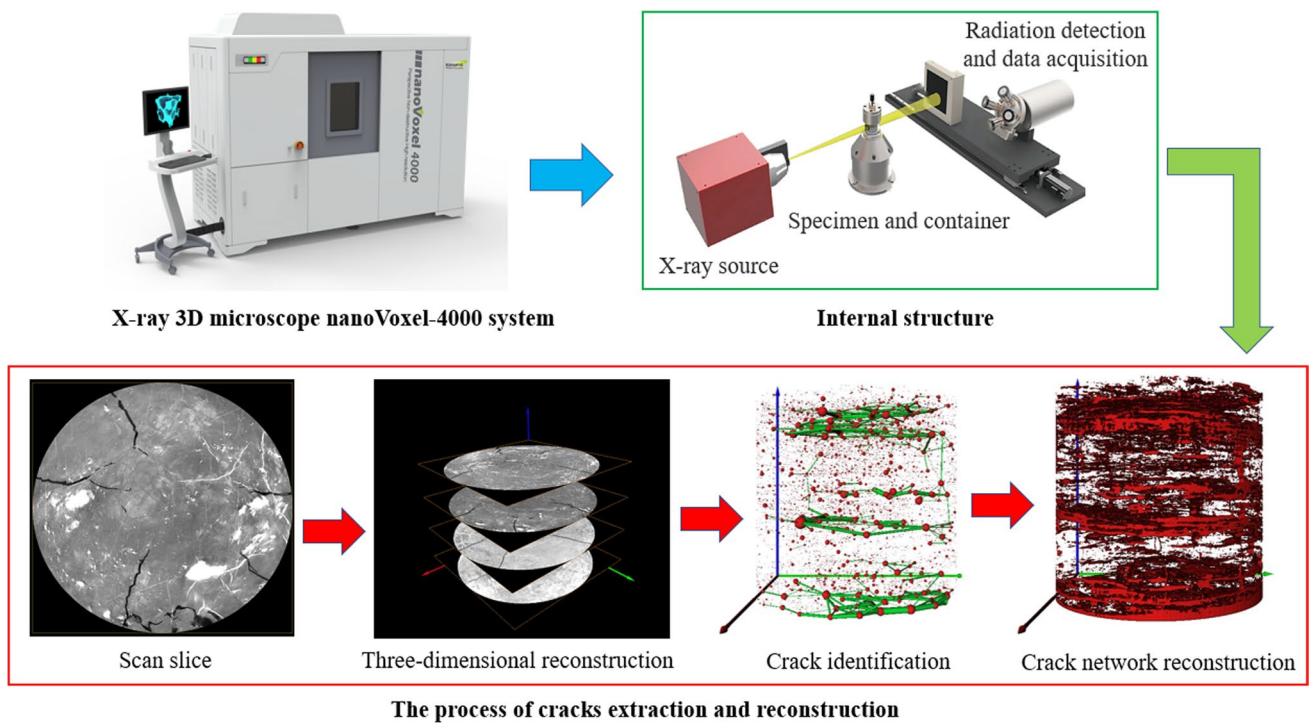


Fig. 1 CT device and crack network reconstruction process

were stacked layer by layer to form a three-dimensional structure. A total of 1000 16-bit grayscale images with 850×850 pixels were obtained by CT scanning of the entire standard coal specimen. At this time, the cracks were further identified, information about each fracture (length, area, volume, width, angle, etc.) was extracted in three dimensions, and finally, the crack network of the entire specimen was reconstructed (Wu et al. 2021; Yang et al. 2021).

2.2 The analysis of correlations

To establish a quantitative relationship between the mechanical properties (UCS and E) and crack data of the CT image, the coal specimens were scanned using X-ray CT. Then, eight typical specimens were selected to conduct uniaxial compression tests to obtain the UCS and E . The stress–strain curves of the coal specimens are shown in Fig. 2, and the typical four stages (i.e., compaction, elastic stage, yielding and postpeak stage) and brittle failure is evident in each curve (Liu et al. 2018; Wang et al. 2020). Due to the presence of a large number of micropores and cracks, all the specimens showed notable compaction characteristics during initial loading, and then the stress gradually reached the peak value as the strain increased (Liu et al. 2019; Zhao et al. 2023). However, the UCS and E of the specimens were different due to the varied internal crack structures of the specimens.

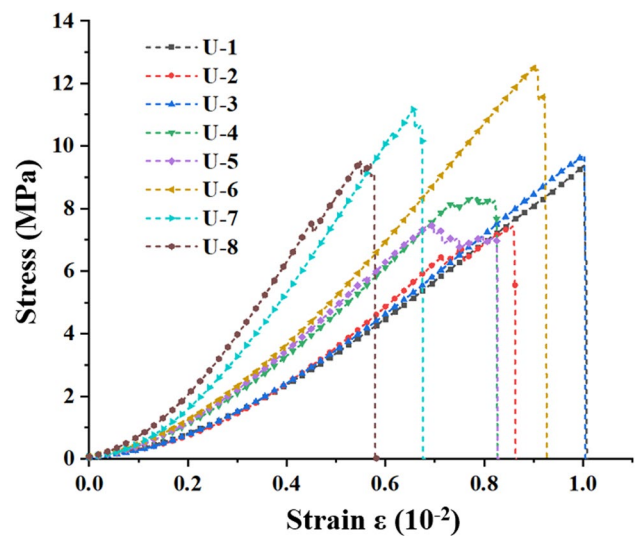
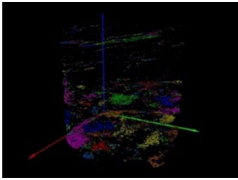
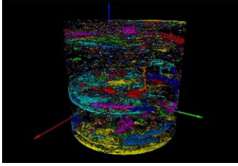
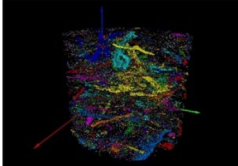
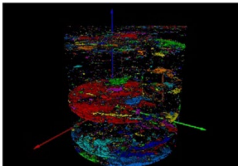
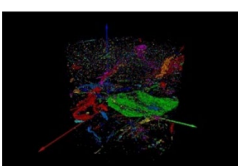
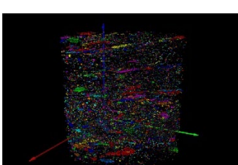
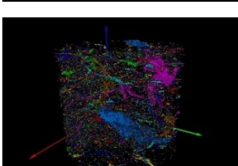
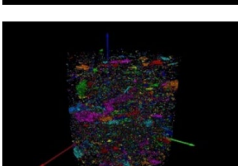


Fig. 2 Comparison of the stress–strain curves of the coal specimens

Table 1 shows the results of the uniaxial compression tests and CT scans. Through the CT scanning image, it can be seen that the interior of the coal specimen is teeming with a large number of randomly distributed cracks. These cracks with different sizes and characteristics greatly affect the stress structure of the specimens, resulting in different mechanical properties, such as UCS and E (Liu et al. 2019; Zhao et al. 2023). However, it is difficult to directly analyze

Table 1 Results of the uniaxial compression test and CT scan

Mark	Crack structure	Porosity (%)	Total number	UCS (MPa)	E_c (GPa)
U-1		0.15	458,617	9.37	0.76
U-2		1.00	2,458,280	7.44	0.72
U-3		0.87	5,095,080	9.71	0.79
U-4		0.54	3,726,483	8.35	0.89
U-5		0.44	585,263	7.47	0.89
U-6		0.24	1,401,641	12.53	1.11
U-7		0.71	243,591	11.21	1.36
U-8		0.35	123,006	9.50	1.42

the relationship between crack characteristics and rock mechanical properties only from the data in Table 1.

The Pearson correlation coefficient (R) is a widely used statistical tool that measures the strength of the relationship between variables (Abubakar et al. 2023; Aladejare

et al. 2022). Therefore, this coefficient is introduced here to analyze the correlation between rock mechanical properties and crack characteristics and is calculated as follows (Cai et al. 2020):

$$R = \frac{\sum_{i=1}^n (X_i - \bar{X})(Y_i - \bar{Y})}{\sqrt{\sum_{i=1}^n (X_i - \bar{X})^2} \sqrt{\sum_{i=1}^n (Y_i - \bar{Y})^2}} \quad (2)$$

where R is the Pearson correlation coefficient between parameters X and Y , n is the number of samples of parameters X and Y , X_i and Y_i are the individual sample points indexed with i , \bar{X} is the sample mean of X_i , and \bar{Y} is the sample mean of Y_i .

The value range of R is between -1 and $+1$. When $R > 0$, the two parameters are positively correlated. Otherwise, they are negatively correlated. Conventionally, the absolute values of R from 0.8 to 1.0 indicate an extremely strong correlation, values ranging from 0.6 to 0.8 indicate a strong correlation, values from 0.4 to 0.6 indicate a moderate correlation, values from 0.2 to 0.4 indicate a weak correlation, and values ranging from 0 to 0.2 indicate a very weak correlation or no correlation (Chen et al. 2022; Su et al. 2020; Zhao et al. 2021).

Correlations between the number of cracks, porosity, and different mechanical parameters (UCS, E) of the coals, calculated according to Eq. (2), are shown in Table 2. It can be seen that the porosity is weakly correlated with UCS and E , reflecting the porosity weakening effect on the strength and stiffness at a lower level. In addition, the number of cracks has almost no effect on UCS but has a relatively strong effect on E , reflecting the weakening effect of the number of cracks on the stiffness. More factors affecting the rock mechanics properties will be analyzed in the following sections.

Numerous studies have shown that the mechanical properties of rocks are significantly affected by porosity and crack geometric parameters (such as crack angle, and length) (Patel and Martin 2020; He et al. 2022; Zhao et al. 2023). Specifically, porosity is closely related to the total number, volume, and area of cracks. Based on the fractal concept, a selection of crack parameters, such as the area, volume, length, and width of the cracks within the specimen, were statistically calculated as variables about the crack parameters (the statistical results are shown in “Appendix A”), and Pearson coefficients R were calculated between the variables and the mechanical parameters of the coal specimens (UCS, E), as shown in Table 3.

Table 2 Correlations between the number of cracks, porosity, and different mechanical parameters of the coals

R	Porosity	The number of cracks
R for UCS	-0.33	-0.18
R for E	-0.25	-0.55

With regard to the variables related to area, the variable S_{\max} had the strongest correlation with the UCS ($R = -0.60$), showing a strong negative correlation. The variable S_{ta} had the weakest correlation with the UCS ($R = -0.35$), showing a weak negative correlation. Additionally, it was discovered that as the statistical threshold was increased, the correlation between the variables associated with area and the UCS also increased, indicating that the dominant crack played a role in weakening strength. Regarding the mechanical parameter E , S_{\max} also had a strong correlation ($R = -0.45$), showing a moderate positive correlation. This indicates that the dominant crack also played an important role in weakening stiffness. Notably, the correlation between E and the area variables decreased as the statistical threshold was increased, until the threshold reached 10 mm^2 , at which point the correlation changed from moderate to weak, which is different from the UCS. These results indicated that small cracks can also weaken stiffness.

Among the volume-related variables, the variable S_{\max} also showed the strongest negative correlation with the UCS ($R = -0.62$), and the correlation between the volume-related variables and the UCS also increased as the statistical threshold increased, which further indicated that the dominant crack played a role in weakening strength. For the mechanical parameter E , S_{\max} displays the strongest correlation ($R = -0.37$) among the volume-related variables but shows a weak correlation. In addition, V_{ta} also showed a weak correlation ($R = -0.37$), while V_1 , V_5 and V_{10} indicated a very weak correlation or no correlation with E .

In terms of length, the variable L_{\max} retained the strongest negative correlation with the UCS ($R = -0.57$), but the absolute values of R between UCS and other length-related variables were below 0.2 and demonstrated a very weak correlation or no correlation. For the mechanical parameter E , L_{ta} displayed the strongest correlation ($R = -0.53$) with the length-related variables, and the correlation between E and the variables related to length decreased as the statistical threshold increased. L_{10} exhibited a very weak correlation or no correlation with E .

For the variables related to width, the variable W_{\max} has the strongest negative correlation with the UCS ($R = -0.58$), and the correlation between other variables about width and UCS varies with the statistical threshold in a pattern consistent with that of area-related variables. For the mechanical parameter E , W_{ta} displays the strongest correlation ($R = -0.55$) among the width-related variables, and the variable W_{\max} also has a relatively strong correlation with E ($R = -0.48$). Notably, the correlation between E and the width-related variables increased as the statistical threshold increased, which is different from the area.

Previous studies have indicated that the crack angle has a significant effect on the mechanical properties of the specimen (Aliha et al. 2010; Tahmasebinia et al. 2018; Zhao et al. 2023).

Table 3 Correlations between different crack parameters and different mechanical parameters of the coals

Area	Area-related variables				
	S_{\max}	S_{ta}	S_1	S_5	S_{10}
R for UCS	-0.60	-0.29	-0.32	-0.35	-0.36
R for E	-0.45	-0.53	-0.44	-0.40	-0.39
Volume	Volume-related variables				
	V_{\max}	V_{ta}	V_1	V_5	V_{10}
R for UCS	-0.62	-0.33	-0.31	-0.34	-0.35
R for E	-0.37	-0.25	-0.02	0.00	0.00
Length	Length-related variables				
	L_{\max}	L_{ta}	L_1	L_5	L_{10}
R for UCS	-0.57	-0.18	0.10	0.05	0.07
R for E	-0.15	-0.54	-0.36	-0.22	0.02
Width	Width-related variables				
	W_{\max}	W_{ta}	W_1	W_5	W_{10}
R for UCS	-0.58	-0.12	-0.40	-0.51	-0.58
R for E	-0.48	-0.55	-0.12	-0.40	-0.51

Note: The variables represented by S_{\max} , V_{\max} , L_{\max} and W_{\max} are the maximum area, maximum volume, maximum length, and maximum width of a single crack within the specimen, respectively; S_{ta} , V_{ta} , L_{ta} and W_{ta} are the sum of the areas, volumes, lengths, and openings of all cracks within the specimen, respectively; S_1 , V_1 , L_1 and W_1 are the sum of all cracks within the specimen with an area greater than 1 mm², the sum of all cracks with an area greater than 1 mm³, the sum of all cracks with a track length greater than 1 mm, and the sum of all cracks with a width greater than 1 mm, respectively; S_5 , V_5 , L_5 and W_5 are the sum of all cracks within the specimen with an area greater than 5 mm², the sum of all cracks with an area greater than 5 mm³, the sum of all cracks with a track length greater than 5 mm, and the sum of all cracks with a width greater than 5 mm, respectively; S_{10} , V_{10} , L_{10} and W_{10} are the sum of all cracks within the specimen with an area greater than 10 mm², the sum of all cracks with an area greater than 10 mm³, the sum of all cracks with a track length greater than 10 mm, and the sum of all cracks with a width greater than 10 mm, respectively

Therefore, the correlations between the maximum crack angle (β_{\max}), area-weighted average angle (β_s), volume-weighted average angle (β_v), and different mechanical parameters (UCS, E) of the coals can be calculated as shown in Table 4. The calculation of the weighted average angle is as follows:

$$\beta_s = \frac{\sum_{i=1}^m \beta_i * S_i}{\sum_{i=1}^m S_i} \quad (3)$$

$$\beta_v = \frac{\sum_{i=1}^m \beta_i * V_i}{\sum_{i=1}^m V_i} \quad (4)$$

Table 4 Correlations between the crack angle and different mechanical parameters of the coals

R	β_{\max}	β_s	β_v
R for UCS	0.54	0.44	0.36
R for E	0.47	0.60	0.61

where m is the number of cracks taken and β_i , S_i and V_i are the individual crack angle, area and volume, respectively.

According to Table 4, β_{\max} shows the strongest negative correlation with the ultimate compressive strength (UCS) ($R=0.54$), followed by β_s ($R=0.44$), which both exhibit a moderate correlation. For the mechanical parameter E , although β_{\max} also shows a moderate correlation ($R=0.47$), its correlation is weaker than β_s ($R=0.60$) and β_v ($R=0.61$). These analyses all indicate that increasing the crack angle weakens the weakening effect of cracks on the strength and stiffness of the specimen.

The correlations between different weighted average angle and mechanical parameters of the coal specimens (UCS, E) were counted for further analysis, as shown in Table 5. It can be seen that as the statistical threshold increased, there was a noticeable increase in the correlation between mechanical parameters and area-weighted variables. This correlation continued to be enhanced until the threshold reached 5 mm², at which point it became remarkably close to the β_{\max} . For volume-weighted variables, the correlation between UCS and the variables increased as the statistical threshold was increased, until

Table 5 Correlations between different weighted average angle and different mechanical parameters of the coals

Area-weighted	Area-weighted variables		
	β_{s1}	β_{s5}	β_{s10}
R for UCS	0.47	0.51	0.51
R for E	0.54	0.55	0.56
Volume-weighted	Volume-weighted variables		
	β_{v1}	β_{v5}	β_{v10}
R for UCS	0.48	0.49	0.52
R for E	0.54	0.51	0.52

Note: The variables represented by β_{s1} , β_{s5} and β_{s10} are the area-weighted average angle of cracks within the specimen with an area greater than 1 mm², 5 mm² and 10 mm², respectively; β_{v1} , β_{v5} and β_{v10} are the volume-weighted average angle of cracks within the specimen with a volume greater than 1 mm³, 5 mm³ and 10 mm³, respectively

the threshold reached 10 mm³, at which point it became remarkably close to the β_{max} .

According to the above analysis of the correlation between crack characteristics and rock mechanical properties, it was discovered that as the statistical threshold is increased, the correlation between the variables and the UCS also increases. All the aforementioned analyses indicate that the dominant crack played an important role in weakening both the strength and stiffness. Furthermore, an analysis of Tables 3, 4, and 5 reveals that when the statistical threshold for crack area is set to 5 mm², there is a high level of correlation between various parameters of the crack and mechanical parameters, meaning that cracks larger than 5 mm² have a significant impact on the mechanical parameters.

3 Crack selection and validation of the triaxial test

3.1 The selection of cracks

The internal cracks in the specimens were sorted in order of size, and then, based on the fractal concept, the sorted

cracks were statistically analyzed separately according to single, four, eight, sixteen, and thirty-two cracks. The statistical results are shown in "Appendix B". Subsequently, the correlation between each crack parameter obtained from each statistical method and the rock mechanical properties was calculated separately, as shown in Table 6.

When studying the correlation, to reduce the impact of error and chance, the top three parameters that were most correlated with each of the two rock mechanics properties were selected for marking (three positive and three negative correlations were chosen for each parameter). During the marking process, the correlation level was considered based on the classification of correlation coefficients in Sect. 2.2, and the parameters with lower correlation levels were removed. The parameters that showed a positive correlation with UCS were β_s ($R=0.58$) for eight cracks, β_s ($R=0.54$) for single cracks, β_v ($R=0.54$) for sixteen cracks, and β_s ($R=0.54$) for thirty-two cracks, and they all showed moderate correlations. The parameters that showed a negative correlation with UCS were V_{ta} ($R=-0.62$), S_{ta} ($R=-0.60$), and W_{ta} ($R=-0.58$), which all showed a strong correlation. W_{ta} showed a moderate correlation and should be removed during marking. The parameters that showed a positive correlation with E were β_s ($R=0.59$) for thirty-two cracks, β_s ($R=0.58$) for sixteen cracks, and β_v ($R=0.56$) for sixteen and thirty-two cracks. The parameters that showed a negative correlation with E were W_{ta} ($R=-0.48$), S_{ta} ($R=-0.45$), and V_{ta} ($R=-0.37$), which all showed moderate correlations. V_{ta} showed a weak correlation with E and should be removed during marking.

Finally, a statistical analysis was conducted on the parameters marked, and it was found that the parameters marked the most were S_{ta} for single cracks and β_s for 16-fold and thirty-twofold cracks, which were marked twice each. This indicates that these parameters have a strong impact on both UCS and E . Additionally, we found that the β and β_v parameters for all statistical methods had correlation coefficients of over 0.4 with the rock mechanics properties, which is not the case for other parameters. This indicates that the angle has a strong impact on the rock mechanics properties, which is consistent with the research of Tahmasebinia

Table 6 Correlations between different crack parameters and different mechanical parameters of the coals

Parameter	Single cracks		Four cracks		Eight cracks		Sixteen cracks		Thirty-two cracks	
	UCS	E	UCS	E	UCS	E	UCS	E	UCS	E
L_{ta}	-0.57	-0.15	0.00	0.39	0.06	0.39	0.05	0.31	0.01	0.27
W_{ta}	-0.58	-0.48	-0.49	-0.33	-0.46	-0.32	-0.45	-0.32	-0.44	-0.33
S_{ta}	-0.60	-0.45	-0.34	-0.24	-0.31	-0.19	-0.30	-0.18	-0.29	-0.17
V_{ta}	-0.62	-0.37	-0.47	-0.14	-0.40	-0.03	-0.36	0.02	-0.34	0.05
β_s	0.54	0.47	0.53	0.51	0.58	0.55	0.54	0.58	0.54	0.59
β_v	0.54	0.47	0.52	0.50	0.50	0.54	0.49	0.56	0.49	0.56

et al. (2018) and Zhao et al. (2023). When comparing the number of parameters marked under different statistical methods, the parameters were marked the most when the statistical methods were single cracks. This further indicates that dominant cracks play a crucial role in affecting the rock mechanics properties. Additionally, sixteen and thirty-two cracks were also marked three times each, indicating that using these statistical methods can also significantly improve the correlation between each parameter of cracks and the rock mechanics properties. This may imply that in future studies on rock masses with complex cracks, in addition to analyzing the parameters of the largest cracks in focus, the geometric parameters of at least 16 cracks should be used as statistics for further analysis or physical reproduction using 3D printing.

3.2 Validation of the triaxial test

To further verify the effectiveness of the conclusions obtained from the abovementioned research in triaxial tests that are closer to the conditions of real coal masses, two specimens were selected from the Liangbaosi coal mine and numbered TC-1 and TC-2 for subsequent triaxial tests. Referring to the ultimate strengths of the specimens in Sect. 2.2 that were determined from uniaxial tests, the confining pressure in the triaxial test was set at 5.0 MPa. The confining pressure increases to the expected value at a constant rate of 0.025 MPa/s. The displacement loading mode with a speed of 0.01 mm/s was used in the axial direction (Chen et al. 2021; Mishra and Vermaet 2015; Pang et al. 2014).

According to the conclusion of the previous section, CT scans were performed on the specimens before and after the triaxial test, and the largest 16 cracks were extracted for statistics (“Appendix C”), which were then analyzed in conjunction with the test results. Finally, the CT scanning images before and after testing (Fig. 3), the statistical results of cracks before and after the test (Table 7), and the stress–strain curves of TC-1 and TC-2 were obtained (Fig. 4).

In the previous section, it was found that S_{\max} and β_s had a large correlation with rock mechanics properties (UCS, E). Therefore, in this section a statistical analysis is performed on these two parameters, as shown in Table 7, and UCS and E are also added for comparison. By comparing the S_{\max} and β_s of TC-1 and TC-2 before testing, it was found that the S_{\max} of TC-1 was 3.41 times that of TC-2, and the β_s values of TC-1 were significantly smaller than those of TC-2. By comparing the rock mechanics properties, it was determined that the UCS and E of TC-1 were significantly smaller than those of TC-2. These comparisons indicate that there is also a negative correlation between S_{\max} and UCS and E in triaxial testing and a positive correlation between

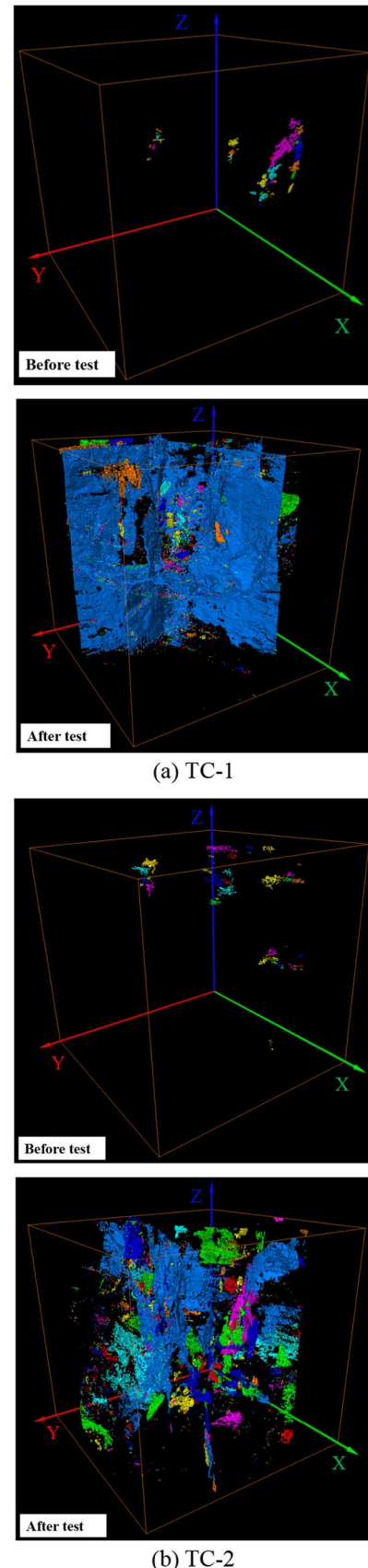


Fig. 3 Changes in the internal cracks in specimens before and after the triaxial compression test

Table 7 Results of the triaxial compression test and statistical crack parameters

Item	Porosity (%)	S_{\max} (mm ²)	β_s (°)	UCS (MPa)	E (GPa)
TC-1 before test	0.0074	60.70	77.29	10.68	0.68
TC-1 after test	1.32	11,300.00	78.50		
TC-2 before test	0.0048	17.80	82.84	12.54	1.08
TC-2 after test	0.43	3,300.00	51.94		

β_s and UCS and E , which is completely consistent with the rules discovered in the uniaxial test.

Table 7 also statistically analyzes the porosity changes before and after the triaxial tests, as well as the two key parameters (S_{\max} and β_s). The β_s values of TC-1 did not change greatly before and after the test, while those of TC-2 changed significantly (i.e., the β_s of TC-2 decreased from 82.84° to 51.94°). Additionally, the S_{\max} of TC-1 after testing is larger than that of TC-2, which is 3.4 times that of TC-2. These analyses indicate that the failure of TC-1 is mainly due to instability and failure after the propagation of cracks, and TC-2 exhibits more damage than TC-1 after the test, which can also be seen from the CT scanning images (Fig. 3). Further analysis will be conducted based on the stress–strain curves and electron microscopy scanning images.

It is observed that the damage to coal specimens occurs in four different stages following loading. These four stages have different deformation characteristics, and the specific results of the analysis are as follows:

Stage I: The compaction stage. Stage I begins from the start point of the stress to point A. As the load continues to increase, the axial and volumetric strains show positive growth, which means that the specimens are axially compressed while their volume decreases. However, it can be seen from the radial strain–stress curve that the radial strain is continuously decreasing, but the magnitude is relatively small. This indicates that during Stage I, the pores and cracks inside the specimen are compacted, and no significant damage is caused. The larger porosity of TC-1 results in a longer duration for this stage compared to TC-2.

Stage II: The crack initiation and steady expansion stage. This stage starts from stress point A, goes to point B1, and then reaches point B2. The axial strain continues to increase, but the volumetric strain starts to decrease continuously. The decrease in radial strain starts to increase, which indicates that the specimen is starting to crack and experience steady expansion. During the loading process,

the specimen is subjected to both strain hardening and strain softening, and these two mechanisms compete with each other (Carpinteri et al. 2006; Zhao et al. 2023). It is noteworthy that TC-2 exhibits a longer duration during this stage and has a smoother ascent of the stress–strain curve compared to TC-1. According to “Appendix C”, the angles of the four largest cracks in the TC-2 specimen are 86.89°, 87.49°, 88.03°, and 89.92°, which are very close to the direction of primary cracks in rock materials during compression (primary cracks, as tensile cracks, usually propagate in a stable manner toward the direction of maximum compression) (Bobet and Einstein 1998; Sagong and Bobet 2002). The similarity in direction facilitates the smooth expansion of cracks.

Stage III: The accelerated destruction stage. This stage starts from stress point B2, goes to point C1, and then reaches point C2. The stress–strain curves begin to depart from the linear behavior, and the volumetric strain and radial strain start to accelerate. This indicates that the specimen enters the stage of accelerated destruction, in which dilatancy deformation and rupture become dominant (Sondergeld and Estey. 1981). Due to the stable propagation of the cracks in the CT-2 specimen toward the direction of maximum compression, this stage lasts for a shorter duration compared to CT-1.

Stage IV: The postpeak stage. This stage starts from stress point B2 and lasts until the stress drops. CT-1 experienced multiple small stress releases in Stage II and Stage III, so its stress–strain curve slumped slowly. However, significant decreases in volumetric strain and radial strain indicate that the specimen has undergone instability and failure due to the propagation of the cracks, which can also be seen in the CT scanning images after the CT-1 test (Fig. 3a). In contrast, CT-2 experienced no significant stress releases in the early stage, and large stress releases only occurred after the stress reached its peak. As a result, the stress–strain curve of CT-2 dropped more quickly, and CT scanning images after its destruction (Fig. 3b) show that specimen CT-2 is more broken than CT-1 inside.

Samples were taken near the main crack of specimens TC-1 and TC-2 after testing to study the micromorphology characteristics of the fracture surface. The samples were analyzed with an APREO electron microscopy scanning system from the FEI Corporation to obtain the micromorphology images of the coal samples, and an accelerating voltage of 2 kV was used in this study.

The typical micromorphology images of TC-1 and TC-2 near the main fractures are shown in Fig. 5. The typical features of the coal samples near the TC-1 main fracture show that most cracks are deflected along the grain boundaries, resulting in a sharp angular edge, and the overall fracture surface appears to be rougher, which is referred to as a typical intergranular (IG) fracture (Mendhe et al. 2018;

Wang et al. 2023). In contrast, the typical features of the coal samples near the TC-2 main fracture show that the overall fracture surface is relatively smoother. Locally, the boundaries of mineral grains are incomplete, and the surfaces have scratches sliding along the fracture surface, which is referred to as a typical transgranular (TG) fracture (Mahanta et al. 2017; Zhu et al. 2023). IG fractures and TG fractures are related to the energy stored before the sample breaks. IG fractures are caused by less energy consumption during the fracture process, while TG fractures are caused by more energy consumption during the fracture process (Abdollahi et al. 2012; Zhang et al. 2023; Zhou et al. 2022). TC-2 experienced no significant stress releases in the early stage, and large stress releases only occurred after the stress reached its peak, resulting in more energy consumption during the fracture process, which caused more TG fractures to occur, which is completely consistent with the trend of the stress–strain curves.

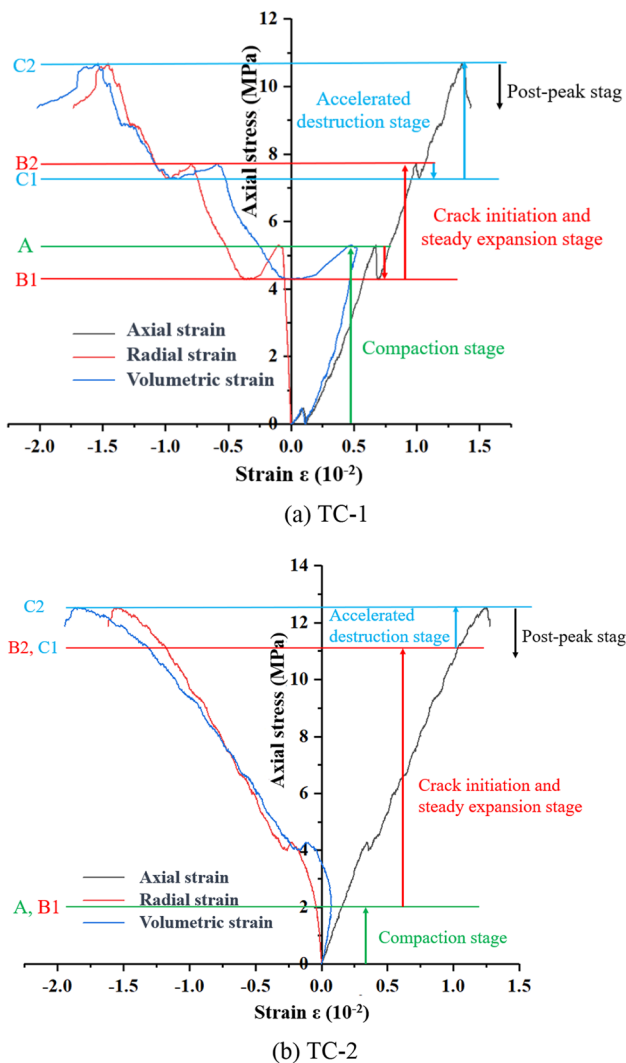
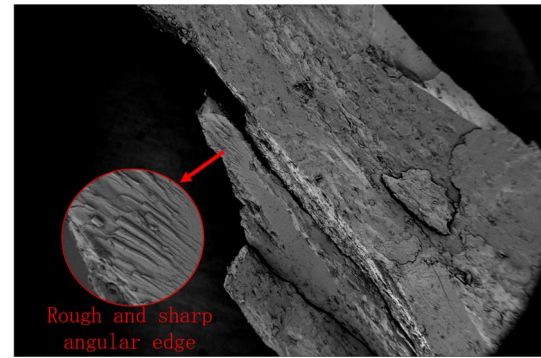
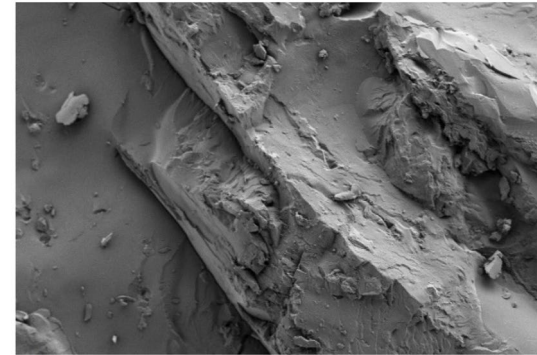


Fig. 4 Stress–strain curves of triaxial compression



(a) TC-1



(b) TC-2

Fig. 5 Microstructure of coal after triaxial compression failure

4 Discussion

It is clear that a deep understanding of the relationship of crack geometric parameters and rock mechanics properties in cracked rock is of great importance to the design of engineering rock mass structures. Currently, 3D printing has been proven to be a powerful technique for simulating rocks and has advantages in replicating complex cracks (Ge et al. 2021; Niu et al. 2023). However, due to the limitations of machine accuracy, 3D printing still has some limitations in replicating small defects, such as microcracks and micropores, which will be a challenge for mechanical experimental research on complex crack rocks. Determining the optimal threshold value will provide a scope for 3D printing to determine the cracks that need to be reproduced during the process of reproducing complex crack rocks. This is so that the rocks reproduced can preserve the impact of cracks on rock mechanics properties to the greatest extent, thereby making the 3D printing specimens more similar to real rocks.

Although the Pearson coefficient was calculated using only 8 test specimens, a significant number of scholars maintain the belief that it can still yield an accurate correlation in similar scenarios (Chen et al. 2022; Abubakar et al. 2023). Furthermore, the results have been corroborated through triaxial

compression tests. However, the previous studies indicate that significant correlations exist between the parameters, meaning that the effect of one crack geometric parameter on UCS is significantly correlated with other crack geometric parameters (Zhao et al. 2023), which is not taken into account by the Pearson correlation coefficients. Therefore, the findings of this study merely represent an initial exploration into the influence of crack geometric parameters on mechanical properties. To obtain more precise data and establish an accurate functional relationship, additional experimental data are needed, which will be a crucial undertaking.

5 Conclusions

In this paper, CT scanning was used to extract the internal crack network of coal specimens. Based on the crack size and dominant crack number, the parameters of crack area, volume, length, width, and angle were statistically analyzed. The Pearson correlation coefficients between the crack parameters and uniaxial compression rock mechanics properties (UCS, *E*) were calculated to analyze the impact of each parameter, and the results were further verified through triaxial testing. Based on the study results, the following conclusions can be made:

- (1) The UCS and *E* of the specimens changed with the varied internal crack structures of the specimens, porosity was weakly negatively correlated with UCS and *E*, and the number of cracks had almost no effect on UCS but had a relatively strong negative correlation with *E*.
- (2) The crack parameters of area, volume, length and width were all negatively correlated with UCS and *E*. The correlation between the variables and the UCS increased as the statistical threshold increased, and the dominant crack played an important role in weakening strength and stiffness. More specifically, there is a high level of correlation between various parameters of the crack and mechanical parameters when the statistical threshold for crack area is set to 5 mm². Hence, the statistics of geometric parameters of the cracks with an area larger than 5 mm² are suggested for analyzing complex cracked rock mass.
- (3) A method based on Pearson coefficients was used to grade the correlation between crack geometric parameters and rock mechanical properties to determine threshold values. The results indicated a positive correlation between angle-related variables and both UCS and *E*. Increasing the quantity of crack statistics significantly improved this correlation. However, the improvement became insignificant when the number of crack statistics reached 16. Therefore, the statistics of geometric parameters of at least 16 cracks are suggested for analyzing complex cracked rock mass or physical reproduction using 3D printing.

- (4) S_{max} and β_s showed a larger correlation with rock mechanics properties (UCS, *E*), and the two key parameters were also proven to have a significant impact on the mechanics parameters of the specimens under triaxial testing, and this impact was largely consistent with that observed during uniaxial testing.

The results of this study can facilitate further targeted research on mechanical properties of rocks with complex cracks, especially how to accurately and efficiently select a few cracks that may have a significant influence on rock mechanical properties from complex and numerous cracks. Furthermore, additional studies may determine that the results may not be limited to soft rock.

Appendix A: The statistical results for crack parameters

Area	Area-related parameters (mm ²)				
	S_{max}	S_{ta}	S_1	S_5	S_{10}
U-1	845.88	14,685.81	10,077.75	9032.98	8460.10
U-2	28,334.80	73,835.90	53,163.66	50,303.61	48,880.26
U-3	3911.41	94,330.96	46,343.74	36,071.98	31,615.29
U-4	9416.49	59,936.61	23,765.05	18,078.70	16,419.19
U-5	8788.78	24,592.37	12,634.16	9935.48	9,384.96
U-6	3536.15	24,754.35	11,483.51	8607.85	7998.92
U-7	4045.01	30,939.80	24,818.53	22,748.86	21,731.57
U-8	2358.67	16,305.42	13,034.60	11,773.82	11,151.17
Volume	Volume-related parameters (mm ³)				
	V_{max}	S_{ta}	V_{max}	S_5	V_{max}
U-1	26.56	293.05	169.32	117.23	57.85
U-2	1083.13	1954.63	1564.91	1440.82	1406.73
U-3	123.15	1705.32	580.36	365.81	276.65
U-4	259.05	1061.34	394.74	359.22	352.50
U-5	524.82	856.00	529.70	524.82	524.82
U-6	120.39	474.04	231.59	211.68	199.74
U-7	247.05	1390.93	1107.43	986.01	928.39
U-8	132.21	692.28	526.74	453.75	416.92
Length	Length-related parameters (mm)				
	L_{max}	S_{ta}	L_{max}	S_5	L_{max}
U-1	31.42	37,628.39	2520.35	863.85	474.51
U-2	64.94	181,555.02	5357.39	1239.20	539.65
U-3	48.12	401,078.12	16,235.19	2052.28	639.68
U-4	48.77	284,793.19	10,130.30	857.79	246.93
U-5	53.34	60,859.60	3715.18	133.63	53.34
U-6	40.77	104,179.19	7487.53	473.58	131.55
U-7	47.48	33,337.85	4187.53	1180.08	617.98
U-8	47.32	17,751.73	2655.85	774.77	431.12

Width	Width-related parameters (mm)				
	W_{max}	S_{ta}	W_{max}	S_5	W_{max}
U-1	6.44	19,302.43	137.26	12.77	0.00
U-2	48.89	101,646.77	343.07	104.75	78.49
U-3	11.36	213,420.48	664.67	57.74	11.36
U-4	21.11	152,990.73	210.60	43.49	21.11
U-5	21.70	30,633.01	70.27	21.70	21.70
U-6	14.14	51,779.02	71.41	14.14	14.14
U-7	10.28	17,797.00	215.50	49.30	10.28
U-8	7.33	9049.55	120.54	18.91	0.00

Appendix B: Crack parameter statistics of under different statistical methods

Single cracks	Parameters for single cracks					
	L_{ta} (mm)	W_{ta} (mm)	S_{ta} (mm ²)	V_{ta} (mm ³)	β_s (°)	β_v (°)
U-1	31.42	6.44	845.88	26.56	77.24	77.24
U-2	64.94	48.89	28,334.80	1083.13	47.41	47.41
U-3	48.12	11.36	3911.41	123.15	85.37	85.37
U-4	48.77	21.11	9416.49	259.05	78.78	78.78
U-5	53.34	21.70	8788.78	524.82	71.99	71.99
U-6	40.77	14.14	3536.15	120.39	77.24	77.24
U-7	47.48	10.28	4045.01	247.05	82.28	82.28
U-8	47.32	7.33	2358.67	132.21	82.28	82.28

Four cracks	Parameters for four cracks					
	L_{ta} (mm)	W_{ta} (mm)	S_{ta} (mm ²)	V_{ta} (mm ³)	β_s (°)	β_v (°)
U-1	99.06	17.01	2317.00	67.42	78.36	78.47
U-2	163.00	77.04	37,104.00	1358.40	55.55	54.43
U-3	74.90	16.88	2372.00	52.38	81.96	81.95
U-4	139.98	38.75	11,998.00	341.50	79.31	79.45
U-5	75.49	27.69	172.20	529.68	72.20	71.99
U-6	101.13	24.16	6039.00	199.40	76.34	75.97
U-7	170.40	29.97	10,900.00	610.30	82.28	82.31
U-8	134.57	19.80	5017.76	271.81	82.07	82.09

Eight cracks	Parameters for eight cracks					
	L_{ta} (mm)	W_{ta} (mm)	S_{ta} (mm ²)	V_{ta} (mm ³)	β_s (°)	β_v (°)
U-1	185.55	31.61	3454.00	98.88	79.36	79.39
U-2	256.27	104.37	39,321.00	1413.47	56.76	55.24
U-3	122.80	35.15	3545.00	78.60	77.56	77.52
U-4	210.60	57.05	12,987.00	366.66	78.99	79.02
U-5	97.77	33.66	276.94	533.24	67.25	71.89
U-6	148.30	34.92	6709.00	219.25	75.48	75.04

Eight cracks	Parameters for eight cracks					
	L_{ta} (mm)	W_{ta} (mm)	S_{ta} (mm ²)	V_{ta} (mm ³)	β_s (°)	β_v (°)
U-7	285.20	46.60	14,113.00	800.10	81.69	81.39
U-8	223.87	36.10	7049.51	391.52	81.77	81.81

Sixteen cracks	Parameters for sixteen cracks					
	L_{ta} (mm)	W_{ta} (mm)	S_{ta} (mm ²)	V_{ta} (mm ³)	β_s (°)	β_v (°)
U-1	318.99	54.18	5054.00	137.88	78.91	78.92
U-2	374.38	133.19	41,004.00	1456.73	57.49	55.79
U-3	197.63	60.85	5027.00	110.52	76.36	76.33
U-4	287.86	80.04	13,754.00	386.81	78.31	78.34
U-5	136.90	43.60	436.22	537.93	70.15	71.92
U-6	204.24	44.46	7153.70	230.91	75.02	74.40
U-7	412.30	72.45	16,203.00	921.01	81.59	81.31
U-8	326.09	56.04	8429.20	451.82	81.33	81.47

Thirty-two cracks	Parameters for thirty-two cracks					
	L_{ta} (mm)	W_{ta} (mm)	S_{ta} (mm ²)	V_{ta} (mm ³)	β_s (°)	β_v (°)
U-1	492.87	84.81	6233.10	163.60	78.47	78.60
U-2	543.33	166.84	42,940.10	1506.77	58.44	56.54
U-3	302.86	91.42	6222.90	137.08	76.63	76.58
U-4	409.19	108.07	14,503.20	403.11	78.10	78.12
U-5	205.72	59.74	624.56	543.44	70.31	71.89
U-6	280.22	60.59	7513.70	241.45	74.96	74.19
U-7	586.86	101.30	17,856.80	1010.63	81.36	81.06
U-8	488.76	81.25	9425.92	495.15	81.30	81.44

Appendix C: Crack parameters before and after TC-1 and TC-2 tests

Crack number	Crack parameters of TC-1 before test				
	Length (μm)	Width (μm)	Area (μm ²)	Volume (μm ³)	Angle (°)
1	10,650.5	2376.97	6.07×10^7	1.81×10^9	74.04
2	5533.21	646.94	1.87×10^7	5.98×10^8	88.22
3	5286.81	1933.8	1.86×10^7	5.70×10^8	70.65
4	6837.73	1630.57	1.86×10^7	5.24×10^8	75.5
5	5406.29	1530.13	1.71×10^7	5.04×10^8	83.02
6	5256.89	888.11	1.44×10^7	4.27×10^8	82.63
7	4012.27	1117.91	1.10×10^7	3.16×10^8	47.18
8	2790.09	1029.65	6.79×10^6	2.26×10^8	87.83
9	4050.09	922.99	7.12×10^6	2.10×10^8	77.18
10	3521.47	751.69	6.60×10^6	1.91×10^8	75.96
11	3396.98	607.82	6.82×10^6	1.90×10^8	86.91

Crack number	Crack parameters of TC-1 before test				
	Length (μm)	Width (μm)	Area (μm ²)	Volume (μm ³)	Angle (°)
12	2903.15	795.04	6.14 × 10 ⁶	1.76 × 10 ⁸	89.04
13	2189.02	1154.65	4.57 × 10 ⁶	1.31 × 10 ⁸	82.52
14	3763.22	654.72	3.89 × 10 ⁶	1.13 × 10 ⁸	80.23
15	3253.42	748.95	3.64 × 10 ⁶	1.00 × 10 ⁸	87.33
16	1701.7	778.66	2.82 × 10 ⁶	8.03 × 10 ⁷	89.53

Crack number	Crack parameters of TC-1 after test				
	Length (μm)	Width (μm)	Area (μm ²)	Volume (μm ³)	Angle (°)
1	65,650.7	42,318.9	1.13 × 10 ¹⁰	1.11 × 10 ¹²	78.92
2	23,113.5	3636.88	4.35 × 10 ⁸	3.47 × 10 ¹⁰	85.95
3	23,514.1	4766.63	2.85 × 10 ⁸	1.70 × 10 ¹⁰	58.31
4	7883.62	1275.65	5.65 × 10 ⁷	5.23 × 10 ⁹	54.50
5	8534.15	2373.38	8.13 × 10 ⁷	4.34 × 10 ⁹	79.04
6	5859.82	836.12	2.62 × 10 ⁷	1.87 × 10 ⁹	61.37
7	4725.8	3154.76	3.55 × 10 ⁷	1.74 × 10 ⁹	53.29
8	8938.48	2088.57	4.35 × 10 ⁷	1.55 × 10 ⁹	88.88
9	6845.37	1002.47	2.53 × 10 ⁷	1.32 × 10 ⁹	86.26
10	5073.99	2140.12	2.05 × 10 ⁷	1.01 × 10 ⁹	86.48
11	2999.52	898.61	1.18 × 10 ⁷	8.77 × 10 ⁸	75.60
12	7143.73	868.59	2.15 × 10 ⁷	8.28 × 10 ⁸	87.23
13	6641.26	757.54	2.49 × 10 ⁷	7.81 × 10 ⁸	81.02
14	4836.69	999.96	2.17 × 10 ⁷	7.03 × 10 ⁸	53.61
15	4128.56	708.72	1.61 × 10 ⁷	6.76 × 10 ⁸	72.14
16	3507.83	776.68	1.20 × 10 ⁷	6.14 × 10 ⁸	85.39

Crack number	Crack parameters of TC-2 before test				
	Length (μm)	Width (μm)	Area (μm ²)	Volume (μm ³)	Angle (°)
1	6170.77	1435.67	1.78 × 10 ⁷	4.98 × 10 ⁸	86.89
2	4107.71	1470.16	1.33 × 10 ⁷	4.25 × 10 ⁸	87.49
3	6477.08	1289.66	1.47 × 10 ⁷	4.23 × 10 ⁸	88.03
4	6920.79	1650.37	1.44 × 10 ⁷	4.00 × 10 ⁸	89.92
5	4496.12	1213.29	1.16 × 10 ⁷	3.39 × 10 ⁸	76.72
6	4492.46	1153.69	1.06 × 10 ⁷	3.20 × 10 ⁸	77.9
7	4840.98	1347.54	8.80 × 10 ⁶	2.81 × 10 ⁸	85.07
8	3947.94	798.04	8.99 × 10 ⁶	2.73 × 10 ⁸	74.93
9	2697.2	824.57	5.20 × 10 ⁶	1.55 × 10 ⁸	81.52
10	2346.15	843.44	4.19 × 10 ⁶	1.45 × 10 ⁸	78.27
11	2339.1	538.7	3.24 × 10 ⁶	1.16 × 10 ⁸	80.29
12	2215.83	471.91	4.17 × 10 ⁶	1.11 × 10 ⁸	60.61
13	3372.05	666.55	3.57 × 10 ⁶	9.78 × 10 ⁷	83.88
14	3542.69	731.64	2.99 × 10 ⁶	8.48 × 10 ⁷	85.59
15	2059.6	476.64	2.65 × 10 ⁶	7.70 × 10 ⁷	88.23
16	2330.32	503.57	2.40 × 10 ⁶	6.80 × 10 ⁷	67.6

Crack number	Crack parameters of TC-2 after test				
	Length (μm)	Width (μm)	Area (μm ²)	Volume (μm ³)	Angle (°)
1	52,764.6	29,443.1	3.30 × 10 ⁹	1.89 × 10 ¹¹	63.34
2	36,729.8	8828.59	5.54 × 10 ⁸	3.23 × 10 ¹⁰	14.35
3	28,620.5	3127.85	4.00 × 10 ⁸	2.17 × 10 ¹⁰	9.85
4	20,269.9	13,194.8	4.27 × 10 ⁸	2.00 × 10 ¹⁰	23.52
5	20,993.5	7844.68	3.50 × 10 ⁸	1.69 × 10 ¹⁰	85.58
6	12,075.8	3837.24	1.23 × 10 ⁸	6.83 × 10 ⁹	68.97
7	10,997.9	2749.35	1.23 × 10 ⁸	5.23 × 10 ⁹	76.18
8	11,581.7	2344.8	1.08 × 10 ⁸	4.98 × 10 ⁹	49.61
9	17,682.2	3550.51	8.09 × 10 ⁷	4.83 × 10 ⁹	89.28
10	12,999.3	3351.25	8.60 × 10 ⁷	3.89 × 10 ⁹	14.66
11	8605.07	2001.47	5.31 × 10 ⁷	2.58 × 10 ⁹	9.19
12	8128.58	1431.56	4.72 × 10 ⁷	2.45 × 10 ⁹	15.98
13	7049.97	1229.86	4.26 × 10 ⁷	2.44 × 10 ⁹	83.39
14	8175.59	3077.94	4.79 × 10 ⁷	2.43 × 10 ⁹	48.88
15	8850.25	1510.56	4.30 × 10 ⁷	2.24 × 10 ⁹	21.83
16	11,452	1389.3	6.61 × 10 ⁷	2.20 × 10 ⁹	49.53

Acknowledgements This study was financially supported by the Young Scientist Project of National Key Research and Development Program of China (2021YFC2900600), National Natural Science Foundation of China (52074166) and Shandong Province (ZR2021YQ38).

Availability of data materials Data used to support the results of this study can be found in this manuscript text.

Declarations

Competing interest The authors declare that they have no known competing financial interests or personal relationships that could have appeared to influence the work reported in this paper.

Open Access This article is licensed under a Creative Commons Attribution 4.0 International License, which permits use, sharing, adaptation, distribution and reproduction in any medium or format, as long as you give appropriate credit to the original author(s) and the source, provide a link to the Creative Commons licence, and indicate if changes were made. The images or other third party material in this article are included in the article’s Creative Commons licence, unless indicated otherwise in a credit line to the material. If material is not included in the article’s Creative Commons licence and your intended use is not permitted by statutory regulation or exceeds the permitted use, you will need to obtain permission directly from the copyright holder. To view a copy of this licence, visit <http://creativecommons.org/licenses/by/4.0/>.

References

- Abdollahi A, Arias I (2012) Numerical simulation of intergranular and transgranular crack propagation in ferroelectric polycrystals. *Int J Fract* 174:3–15
- Abubakar R, Adomako-Ansah K, Marfo SA, Fenyi C, Owusu JA (2023) Integrated geochemical and statistical evaluation of the source rock potential in the deep-water, Western Basin of Ghana. *J Petrol Sci Eng* 220:111164
- Aladejare AE, Ozoji T, Lawal AI, Zhang Z (2022) Soft computing-based models for predicting the characteristic impedance of igneous rock from their physico-mechanical properties. *Rock Mech Rock Eng* 55(7):4291–4304
- Aliha MRM, Ayatollahi MR, Smith DJ, Pavier MJ (2010) Geometry and size effects on fracture trajectory in a limestone rock under mixed mode loading. *Eng Fract Mech* 77(11):2200–2212. <https://doi.org/10.1016/j.engfracmech.2010.03.009>
- Bao H, Zhang G, Lan H, Yan C, Xu J, Xu W (2020) Geometrical heterogeneity of the joint roughness coefficient revealed by 3D laser scanning. *Eng Geol* 265:105415
- Bobet A, Einstein HH (1998) Fracture coalescence in rock-type materials under uniaxial and biaxial compression. *Int J Rock Mech Min Sci* 35(7):863–888. [https://doi.org/10.1016/S0148-9062\(98\)00005-9](https://doi.org/10.1016/S0148-9062(98)00005-9)
- Cai J, Xu K, Zhu Y, Hu F, Li L (2020) Prediction and analysis of net ecosystem carbon exchange based on gradient boosting regression and random forest. *Appl Energy* 262:114566
- Cao RH, Cao P, Lin H, Pu CZ, Ou K (2016) Mechanical behavior of brittle rock-like specimens with pre-existing fissures under uniaxial loading: experimental studies and particle mechanics approach. *Rock Mech Rock Eng* 49(3):763–783. <https://doi.org/10.1007/s00603-015-0779-x>
- Carpinteri A, Lacidogna G, Niccolini G (2006) Critical behaviour in concrete structures and damage localization by acoustic emission. *Key Eng Mater* 312(2006):305–310. <https://doi.org/10.4028/www.scientific.net/KEM.312.305>
- Chen Y, Zuo J, Liu D, Li Y, Wang Z (2021) Experimental and numerical study of coal-rock bimaterial composite bodies under triaxial compression. *Int J Coal Sci Technol* 8:1–17
- Chen X, Feng L, Wang J, Guo S, Xu Y (2022) Cyclic triaxial test investigation on tuffs with different water content at Badantoru Hydropower Station in Indonesia. *Eng Geol* 300:106554
- Cui J, Jiang Q, Li S, Feng X, Zhang Y, Shi YE (2020) Numerical study of anisotropic weakening mechanism and degree of non-persistent open joint set on rock strength with particle flow code. *KSCE J Civ Eng* 24:988–1009
- Gao H, Wang Q, Jiang B, Zhang P, Jiang Z, Wang Y (2021) Relationship between rock uniaxial compressive strength and digital core drilling parameters and its forecast method. *Int J Coal Sci Technol* 8:605–613
- Ge Y, Lin Z, Tang H, Zhao B (2021) Estimation of the appropriate sampling interval for rock joints roughness using laser scanning. *Bull Eng Geol Env* 80:3569–3588
- He M, Zhang Z, Zhu J et al (2022) Correlation Between the constant m of Hoek–Brown criterion and porosity of intact rock. *Rock Mech Rock Eng* 55:923–936. <https://doi.org/10.1007/s00603-021-02718-2>
- Huang X, Yang D, Kang Z (2021) Three-phase segmentation method for organic matter recognition in source rocks via ct images: a case study on oil shale pyrolyzed by steam. *Energy Fuels* 12:35
- Jiang L, Sainoki A, Mitri HS, Ma N, Liu H, Hao Z (2016) Influence of fracture-induced weakening on coal mine gateroad stability. *Int J Rock Mech Min Sci* 88:307–317
- Kong P, Jiang L, Shu J, Sainoki A, Wang Q (2019) Effect of fracture heterogeneity on rock mass stability in a highly heterogeneous underground roadway. *Rock Mech Rock Eng* 52(11):4547–4564
- Li DY, Han ZY, Sun XL, Zhou T, Li XB (2019) Dynamic mechanical properties and fracturing behavior of marble specimens containing single and double flaws in SHPB tests. *Rock Mech Rock Eng* 52(6):1623–1643. <https://doi.org/10.1007/s00603-018-1652-5>
- Liu JJ, Yang M, Wang D, Zhang JH (2018) Different bedding loaded coal mechanics properties and acoustic emission. *Environ Earth Sci* 77(8):1–11. <https://doi.org/10.1007/s12665-018-7504-5>
- Liu SM, Li XL, Li ZH, Chen P, Yang XL, Liu YJ (2019) Energy distribution and fractal characterization of acoustic emission during coal deformation and fracturing. *Measurement* 136:122–131. <https://doi.org/10.1016/j.measurement.2018.12.049>
- Mahanta B, Tripathy A, Vishal V, Singh TN, Ranjith PG (2017) Effects of strain rate on fracture toughness and energy release rate of gas shales. *Eng Geol* 218:39–49
- Mendhe VA, Kumar V, Saxena VK, Bannerjee M, Kamble AD, Singh BD, Samad SK (2018) Evaluation of gas resource potentiality, geochemical and mineralogical characteristics of Permian shale beds of Latehar-Auranga Coalfield, India. *Int J Coal Geol* 196:43–62
- Mishra B, Verma P (2015) Uniaxial and triaxial single and multi-stage creep tests on coal-measure shale rocks. *Int J Coal Geol* 137:55–65
- Niu Q, Jiang LS, Li CA, Zhao Y, Wang QB, Yuan AY (2023) Application and prospects of 3d printing in physical experiments of rock mass mechanics and engineering: materials, methodologies and models. *Int J Coal Sci Technol* 10(1):1–17
- Omori T, Suzuki S, Michibayashi K, Okamoto A (2023) Super-resolution of X-ray CT images of rock samples by sparse representation: applications to the complex texture of serpentinite. *Sci Rep* 13(1):6648
- Otsu N (1979) A threshold selection method from gray-level histograms. *IEEE Trans Syst Man Cybern* 9(1):62–66
- Pang Y, Wang G, Ding Z (2014) Mechanical model of water inrush from coal seam floor based on triaxial seepage experiments. *Int J Coal Sci Technol* 1:428–433
- Patel S, Martin CD (2020) Impact of the initial crack volume on the intact behavior of a bonded particle model. *Comput Geotech* 127:103764
- Sagong M, Bobet A (2002) Coalescence of multiple flaws in a rock-model material in uniaxial compression. *Int J Rock Mech Min Sci* 39(2):229–241. [https://doi.org/10.1016/S1365-1609\(02\)00027-8](https://doi.org/10.1016/S1365-1609(02)00027-8)
- Salamon M, Arzig M, Wellmann PJ, Uhlmann N (2019) Comparison of achievable contrast features in computed tomography observing the growth of a 4h-sic bulk crystal. *Materials* 12(22):3652
- Sondergeld CH, Estey LH (1981) Acoustic emission study of microfracturing during the cyclic loading of Westerly granite. *J Geophys Res Solid Earth* 86(B4):2915–2924. <https://doi.org/10.1029/JB086iB04p02915>
- Su XB, Ji HG, Quan DL, Geng JM, Zhang GG, Gao Y (2020) Relationship between spatial variability of rock strain and b value under splitting condition. *J China Coal Soc* 45(1):239–246
- Tahmasebinia F, Zhang CG, Cambulat I, Vardar O, Saydam S (2018) Computing the damage and fracture energy in a coal mass based on joint density. *Int J Min Sci Technol* 28(5):813–817. <https://doi.org/10.1016/j.ijmst.2018.08.013>
- Wang HY, Wang GD, Zhang GJ, Du F, Ma J (2020) Acoustic emission response characteristics of anthracitic coal under uniaxial compression. *Shock Vib* 2020:8874164. <https://doi.org/10.1155/2020/8874164>
- Wang J, Ren Z, Yang S, Ning J, Zhang S, Bian Y (2023) The influence of the strain rate and prestatic stress on the dynamic mechanical properties of sandstone—a case study from China. *Materials* 16(9):3591

- Wong LNY, Einstein HH (2009) Systematic evaluation of cracking behavior in specimens containing single flaws under uniaxial compression. *Int J Rock Mech Min Sci* 46(2):239–249. <https://doi.org/10.1016/j.ijrmms.2008.03.006>
- Wu Y, Zhang Z, Wang X, Zhu P, Yang X, Jiang L (2021) Study on the physical properties and joint evolution characteristics of three-dimensional reconstructed coal. *Adv Mater Sci Eng* 2021:1–15
- Xie H, Wang JA, Xie WH (1997) Fractal effects of surface roughness on the mechanical behavior of rock joints. *Chaos Solitons Fractals* 8(2):221–252
- Xu X, Bao H, Lan H, Liu C, Xu J, Yan C (2022) Sampling interval-size effects and differential sensitivities of different morphology parameters of rock joint. *J Struct Geol* 155:104530
- Yang YS, Li KY, Zhou H, Tian HY, Cheng W, Zhang ZR et al (2021) Investigation on the relationship between CT numbers and marble failure under different confining pressures. *Rev Adv Mater Sci* 60(1):846–852
- Zhang C, Li D, Ma J, Zhu Q, Luo P, Chen Y, Han M (2023) Dynamic shear fracture behavior of rocks: insights from three-dimensional digital image correlation technique. *Eng Fract Mech* 277:109010
- Zhao R, Zhai Y, Meng F, Li Y, Li Y (2021) Research on interactions among parameters affecting dynamic mechanical properties of sandstone after freeze-thaw cycles. *Eng Geol* 293:106332
- Zhao Y, Ning J, Jiang L, Wang Q, Yuan A (2022) Numerical analysis on the joint weakening effect of rock mass behaviors in tension. *Lithosphere* 10:5324148
- Zhao Y, Jiang L, Li C, Niu Q, Sainoki A, Mitri HS, Ning J (2023) Experimental investigation into the mechanical behavior of jointed soft rock using sand powder 3D printing. *Rock Mech Rock Eng*. <https://doi.org/10.1007/s00603-023-03346-8>
- Zhou Y, You L, Wang S, Ku Z, Fan H, Schmidt D et al (2016) Giant photostriction in organic–inorganic lead halide perovskites. *Nat Commun* 7:11193
- Zhou L, Gao W, Yu L, Zhu Z, Chen J, Wang X (2022) Thermal effects on fracture toughness of cracked straight-through Brazilian disk green sandstone and granite. *J Rock Mech Geotech Eng* 14(5):1447–1460
- Zhu S, Ge D, Jiang F, Wang C, Li D, Shang X, Wang Z (2021) Rock burst mechanism under coupling action of working face square and regional tectonic stress. *Shock Vib* 2021(8):1–11
- Zhu Q, Li D, Li X, Han Z, Ma J (2023) Mixed mode fracture parameters and fracture characteristics of diorite using cracked straight through Brazilian disc specimen. *Theor Appl Fract Mech* 123:103682

Publisher's Note Springer Nature remains neutral with regard to jurisdictional claims in published maps and institutional affiliations.